Int J Adv Manuf Technol (2012) 60:1017–1030
DOI 10.1007/s00170-011-3648-0

ORIGINAL ARTICLE

A hybrid-constrained MOGA and local search method to optimize the load path for tube hydroforming

Honggang An · Daniel E. Green · Jennifer Johrendt

Received: 23 December 2010 / Accepted: 14 September 2011 / Published online: 12 October 2011

Abstract The production of a tubular hydroformed part often requires a combination of internal pressure and axial force at the tube ends to fully form the tube to its specified geometry. A successful hydroforming process requires not only achieving a part that conforms to the design specifications, but also ensures that the part has a reasonably uniform thickness distribution and is free of defects, such as wrinkles, severe thinning, or fractures. The load path design (pressure vs. end feed history) largely determines the robustness of the process and the quality of the finished parts. In this paper, a hybrid constrained optimization method was proposed to solve this type of multi-objective problem by coupling a multi-objective genetic algorithm and a local search. The load path design procedure was developed by considering five objectives: four formability objectives (i.e., to minimize the risk of wrinkling, global and local thinning, and fracture) and a geometric objective (to minimize the corner radius). A Kriging predictor was used to accelerate the computation of genetic operations and generate new feasible solutions. Finite element simulations of the hydroforming process were also used after each generation to accurately evaluate the objectives of the offspring, and solutions with rank 1 were retained throughout all generations. Once the Pareto solutions were obtained by multi-objective genetic algorithm, a local search was carried out in the regions of interest with the assistance of visualization. This optimization method was applied to the hydroforming of a straight tube to create a part with an expanded region with a square cross section; the optimum load path produced a very safe part with a corner radius of only 9.115 mm and a maximum thinning of only 23.9%.

Keywords Tube hydroforming · Load path design · Non-dominated sorting genetic algorithm (NSGA) · Kriging model · Constrained multi-objective genetic algorithm (MOGA) · Local search

H. An (✉) · D. E. Green · J. Johrendt
Department of Mechanical, Automotive and Materials Engineering, University of Windsor,
401 Sunset Ave.,
Windsor, ON N9B3P4, Canada
e-mail: anh@uwindsor.ca

D. E. Green
e-mail: dgreen@uwindsor.ca

J. Johrendt
e-mail: Jennifer@uwindsor.ca

1 Introduction

Tube hydroforming has captured the interest of researchers and engineers for several decades. Today, the hydroforming process is used to produce lightweight products for home use and in the automotive and aerospace industries. However, the efficiency of the hydroforming process largely depends on the given load paths (i.e., internal pressure vs. time and end feed vs. time) which are important to generate high-quality parts and save costs.

The design process can be dramatically improved by utilizing finite element analysis (FEA). For instance, Manabe and Amino [1] proposed to calibrate certain process parameters with the aid of FEA simulations and obtained a better load path. Other studies have proposed integrated optimization tools coupled with numerical analysis to obtain an optimal load path [2–6]. Due to time-consuming simulations, however, attempts to obtain a global optimum are still cumbersome and results are often only found at a local optimum.

Recently, several applications using the response surface methodology (RSM) model for accelerating the optimization process have been proposed for tube hydroforming. Koç et al. [7] presented low-cost RSM models to predict the protrusion height of "T-shaped" hydroformed parts, and the

method was shown to provide an economical prediction and optimization of this height as a function of geometrical parameters subject to thinning of the wall in the protrusion region. Ingarao et al. [8] used the classical weighted sum method and ε-constraint methodology to optimize the process design for Y-tube hydroforming: there were two inputs (the maximum pressure and end force at the calibration stage) and three outputs (tube wall thinning, final unfilled volume, and fillet radius). The moving least squares approximation was used to construct the RSM model. Bonte et al. [9] proposed a sequential approximate optimization (by fitting the metamodel) to optimize the metal forming process. It was applied to minimize the variations in wall thickness of the final product with respect to the initial tube thickness using a load path defined by seven parameters, including the initial tube radius and thickness, the time when axial feeding starts and stops, the amount of axial feeding, the increase in internal pressure, and the coefficient of friction.

It can be noted that most of the optimizations performed in tube hydroforming are still accomplished by considering a single objective, or by transforming a multi-objective problem into a single objective by a weighted sum method; moreover, no more than three objectives have been considered.

The authors have proposed using the normal boundary intersection (NBI) method [10] and a multi-objective genetic algorithm (MOGA) method [11] which couples a Kriging surrogate model to optimize the load path problem with four objectives in order to hydroform a part with a square-shaped cross section. Both methods adopted Pareto optimality; however, the NBI method requires a sequential improvement in RSM model which can only be performed manually. The MOGA method, on the contrary, offers an automatic improvement if needed. Nevertheless, it still needs an improvement in dealing with more than three objectives. That is, due to the larger number of objectives, the predefined Kriging model was not able to reach the desired prediction accuracy for all the objectives at the same time. Moreover, it was noted that the maximum thickness reduction, which is a key factor for evaluating the local thinning, was not considered in the above work. As pointed out by Hughes [12], one concern with the methods described so far is that fitness assignments based on dominance rank (like NSGA-II) often performs poorly when the number of objectives is greater than three or four. Although the accuracy can be improved by adding more sampling points, the prediction error may still affect the constraint handling and the poor results may be amplified through the effect of Pareto drift [13].

This paper presents a methodology to establish a hybrid multi-objective global search and local search utilizing a Kriging surrogate model to accelerate the computation process. In Section 2, the Kriging surrogate model is introduced. In Section 3, a constraint-handling MOGA is described and several improvements for constraint-handling techniques based on NSGA-II are discussed. In Section 4, a hybrid multi-objective global and local search is proposed, where the former deals with a global domain to generate a solution set, and the latter deals with the sub-optimal solution and its nearby domain using a ε-constraint strategy (solved by sequential quadratic programming, SQP). In Section 5, an application is given and the results are presented, followed by conclusions in Section 6.

2 Kriging metamodel

In order to accelerate calculation speed, a variety of surrogate methods have been used to substitute the FEA simulations: polynomial regression [14], radial basis functions [15], artificial neural networks [16], and Kriging models [9]. It is obvious that the allocation of the sample points used to build the approximation is important for the final performance of the surrogate model. Many schemes and criteria have been proposed to allocate a priori the sample points in a convex domain of interest: factorial design, Box–Behnken, Koshal, central composite design, D-optimal and space-filling design. All these efforts have been made to approach the true response surface of actual problems. However, it is practically difficult to conclude which one is most suitable for allocation and reduction of sampling points to reach a desired precision.

A computer simulation is repeatable; however, when an established analytical model based on some limited data is used to predict "new" data, the output becomes uncertain due to the limited information that was used to define the "black box" model. The Kriging technique which originated from the field of spatial statistics was developed to represent such a stochastic variable. The response is modeled as a realization of a regression model and a random process [17]. The Kriging model has been shown to be a global model in contrast to response surfaces which are local models, employing normally distributed basis functions, so both an expected sampling value and variance are obtained for each test point [18].

The universal Kriging model can be expressed as:

$$Y(x) = \sum_{i=1}^{p} \beta_i f_i(x) + Z(x) \tag{1}$$

where the coefficients β_i (i=1,…p) are the regression parameters, $f_i(x)$ (i=1,…p) are known functions of x, and the first part is the known approximation function, and $Z(x)$ is the realization of a stochastic process; while the approximation function of $f(x)$ globally approximates the design space, $Z(x)$ creates "localized" deviations so that the

Kriging model interpolates the n_s sampled data points. $Z(x)$ is a random process with mean zero, variance σ^2 and nonzero covariance:

$$\mathrm{Cov}(w,x) = \sigma_k^2 \rho(\theta, w, x),\ \mathrm{k} = 1, 2, \ldots \mathrm{p}; \tag{2}$$

and σ_k^2 is the process variance of the k^{th} component of the response and $\rho(\theta, w_j, x_j)$ is the correlation model. Here, θ is the unknown correlation parameters used to fit the model that is typically estimated by the maximum likelihood estimation method, and w_j and x_j are the jth components of sample points w and x.

Usually, the stochastic process is stationary, which implies that the correlation $\rho(\theta, w_j, x_j)$ depends only on the distance of w_j and x_j, namely

$$\rho\left(\theta, w_j, x_j\right) = \rho\left(\theta, w_j - x_j\right) \tag{3}$$

A Gaussian correlation function (Eq. 4) and a regression model with polynomial order 2 is typically used.

$$\rho\left(\theta, w_j - x_j\right) = \exp\left[-\sum_{j=1}^{n_v} \theta_j \left|w_j - x_j\right|^2\right] \tag{4}$$

Where n_v is the number of design variables.

Unlike response surfaces, however, the Kriging method has found extremely limited use in hydroforming optimization since its introduction by Sacks et al. [19].

The accuracy of the Kriging response surface model can also be measured by checking the predictability of its response using the prediction error sum of squares (PRESS) and R^2 for prediction ($R_{\mathrm{pred}}{}^2$) [14]. After obtaining the surrogate model, a tenfold cross-validation technique was used to check the fitting performance for the "new" data. The PRESS statistic, $R_{\mathrm{pred}}{}^2$ of the predictor model, and S_{yy} (the total sum of squares) were calculated as:

$$\mathrm{PRESS} = \sum_{i=1}^{p} \left(y_i - \hat{y}_i^*\right)^2 / p \tag{5}$$

$$R_{pred^2} = 1 - \frac{\mathrm{PRESS}}{S_{yy}} \tag{6}$$

$$S_{yy} = y^T y - \frac{\left(\sum_{i=1}^{p} y_i\right)^2}{p} = \sum_{i=1}^{p} y_i^2 - \frac{\left(\sum_{i=1}^{p} y_i\right)^2}{p} \tag{7}$$

where y_i is the actual value, $\hat{y}_i^*$ is the value predicted by the Kriging predictor for the i^{th} testing point, and p is the number of prediction points. The final PRESS is the average of ten cross-validation tests.

3 MOGA and constraint-handling technique

3.1 MOGA

Most engineering problems have several, possibly conflicting, objectives, and therefore, all the objectives cannot generally be simultaneously optimized. For instance, for typical hydroformed components, there are competing objectives; there is a need to reduce the risk of necking/fracture and wrinkling, minimize thinning, while achieving a specified geometry and maintaining a reasonably uniform thickness distribution throughout the part. This constitutes a problem of multiple objectives.

To solve problems with multiple objectives, it is common practice to reduce the problem to a single objective, even though there may exist different conflicting goals (e.g., maximizing formability and minimizing thinning) for the optimization task. As a result, multiple goals are often redefined as a weighted sum objective function, thereby artificially reducing the number of apparently conflicting goals into a single objective. However, the correlation between objectives is usually rather complex and difficult to find. As a consequence, it may be very troublesome to combine different objectives into a single goal function a priori, that is, before alternatives are known.

In order to circumvent the difficulty of selecting a relative weight for each objective (where the correlation between objectives is usually rather complex), a Pareto optimization algorithm (called NSGA-II) which uses a ranking, elitist selection and non-dominated sorting strategy was adopted for this study. The NSGA-II algorithm developed by Deb et al. [20] has been a popular optimization tool in recent years. It adopts an elitism strategy and crowding-distance calculation, which offer a much better spread of solutions and better convergence in most problems near the true Pareto-optimal front compared to the Pareto-archived evolution strategy and the strength-Pareto evolutionary algorithm—two other elitist multi-objective evolutionary algorithms (MOEA) that pay special attention to creating a diverse Pareto-optimal front.

The principle of this algorithm is illustrated in Fig. 1. The Pareto fronts were sorted to different ranks according to a fitness value. After this non-dominated sorting, a crowding distance was calculated for each individual (Fig. 1b). The purpose of assigning a crowding distance value is to generate a series of uniformly distributed Pareto fronts, which helps to maintain better diversity of the population.

Goel et al. [13] noted that in MOEA, the genetic operators may destroy some of the solutions to explore the design space. Introducing elitism in MOEAs alleviates this problem to some extent, but when the number of non-

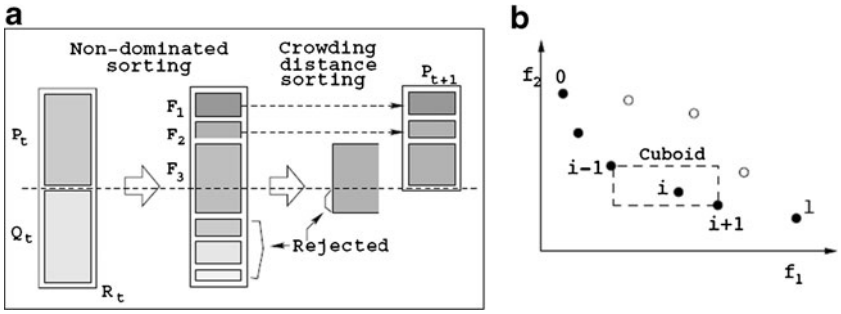

Fig. 1 **a** Schematic of the NSGA-II procedure and **b** the crowding distance calculation (adapted from [20])

dominated solutions in the combined population exceeds the population size, as happens commonly in elitist MOEAs, some of the non-dominated solutions have to be dropped. This problem is referred to as Pareto drift since the Pareto optimal solution is lost, and this may lead to a suboptimal global solution.

Therefore, an archiving strategy is suggested to augment NSGA-II, and is referred to as archiving NSGA-II (NSGA-IIa) [13]. The strategy of NSGA-IIa is to keep all the potential non-dominated solutions in one group during the whole evolution process. In this work, the archive was initialized with all non-dominated solutions inherited from these points of design of experiment, and then complemented with the potential non-dominated solutions from new generations for which fitness functions were calculated by FEA.

3.2 Constraint handling technique

In problems with constraints, it is more difficult to handle violation of the constraints. Most real-world optimization problems have constraints that must be satisfied. Currently, a single-objective genetic algorithm (GA) can employ five different constraint-handling strategies: (1) discarding infeasible solutions, (2) reducing the fitness of infeasible solutions by using a penalty function, (3) if possible, customizing genetic operators to always produce feasible solutions, (4) repairing infeasible solutions, and (5) hybrid methods. Handling of constraints has not been adequately researched for MOGAs [21]. For example, all major multi-objective GA assume problems without constraints.

In general, constraint-handling strategies 1, 3, and 4 are suitable for both single-objective GA and MOGA. However, for the most widely used penalty function strategy, it is not straightforward in MOGA, since it operates on the fitness assignment of an objective value, while for MOGA the fitness assignment is usually based on the non-dominance rank of each solution.

In the constrained NSGA-II, a method using category 4 is described to handle three different non-dominated rankings. Wang and Yin [22] proposed a method of M+1 non-dominated sorting to solve the constraints in engineering design problems (M referred to the number of objectives and 1 referred to the overall constraint violation). Favuzza et al. [23] proposed two crowded comparison operators for constraints handling in the design of an electric distribution network. Deb et al. [20] proposed the constraint-domination concept and a binary tournament selection method based on it, which was called the constrained tournament method. The main advantages of the constrained tournament method are that it requires fewer parameters and it can be easily integrated into multi-objective GA. Seshadri proposed a NSGA-II algorithm programmed with Matlab language [24]. However, the constraint-handling program was not presented.

Hence, in this paper, a hybrid constraint-handling method was proposed (Fig. 2), which aims to utilize the simple operation of the penalty function method and also the tournament selection method. This method can be described as follows:

Step 1 Weeding out the infeasible solutions in the process of generating new children. Evaluate the children using the Kriging model and eliminate those with constraint violations.

Following the initiation of the population, new children were generated through genetic operations (mutation and crossover). The objective values of each child were evaluated with the Kriging predictor. If any of the objective values violated the boundary, then the child was marked with violation. The program continually generated new children until it met the constraints. Although the satisfying of the constraints may be pseudo feasible (since the true objective values probably still violate the boundaries), the violation would remain small so long as a well-established Kriging model was used. Moreover, the operation in step 2 will also help to keep feasible solutions and eventually eliminate infeasible solutions.

Step 2 Ranking by constraint violation (stage 1, Fig. 2)

The comparison mechanism considered here, operated on solutions that have constraint violations and determined a rank for each solution

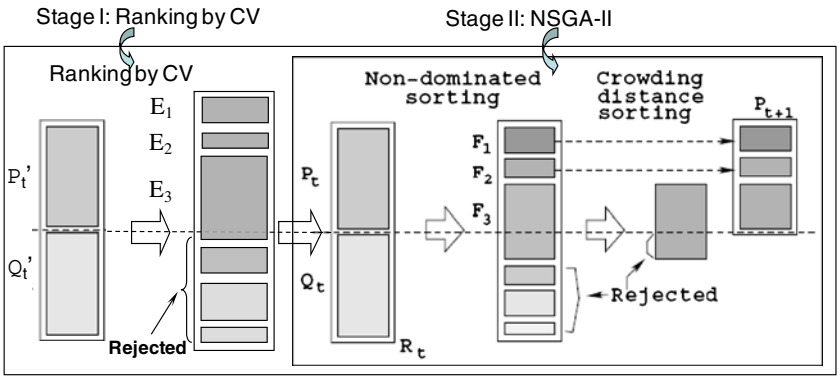

Fig. 2 Constrained NSGA-II algorithm

(see Appendix 1). The constraint violation (CV) values were calculated as:

$$\mathrm{CV} = \sum_{i=1}^{l} [\mathrm{Max}(0, g_i(x))] \tag{8}$$

if there is constraint violation, i.e., $g_i(x)>0$, l is the number of constraints. CV is equal to 0 if there is no constraint violation and $g_i(x)\leq 0$.

Step 3 Ranking of general NSGA-II with non-dominated sorting, crowding distance sorting, and elitism selection (stage 2, Fig. 2)

The algorithm operated in a way that the CV operator was carried out for the population merged from the parent and the offspring. It dominated the operation in the early stages of running the MOGA, but in the later stages, conventional NSGA-II dominated the selection of population for the next generation when the number of the feasible individuals in the merged population had reached the designed population number.

4 A hybrid optimization algorithm coupling global MOGA and local searches

The selection procedure of the MOGA algorithm (Fig. 3) is described as follows:

1. Initialize the parent population P_t'.
2. Create the offspring Q_t' through the crossover and mutation operators. The objective function values are calculated using the Kriging predictor.
3. Check the constraint violation (CV) of each child. If CV>0, randomly generate a new point and evaluate the function by Kriging predictor until the child population is fully filled.
4. Recombine the parent and child populations into a new population $U_t=P_t'UQ_t'$. Carry out non-dominated sorting for CV first. Assign a rank for each individual as E=E1, E2,… (Fig. 2). If the number of U_t exceeds the current population size N, go to step 5, or else go to 6.

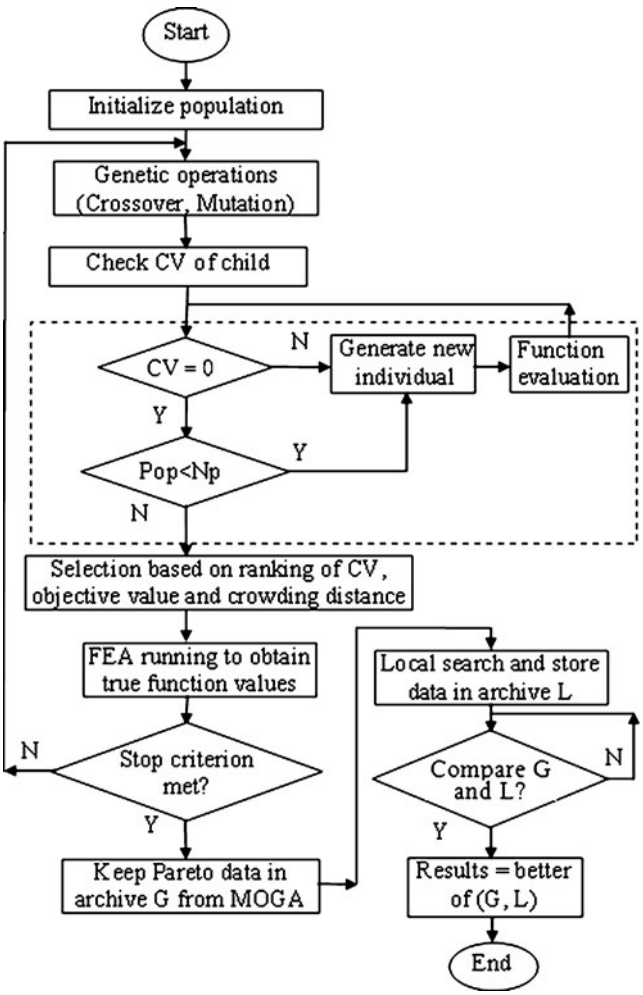

Fig. 3 Flowchart of optimization strategy

5. Recombine the parent and child populations into a new population $R_t=P_tUQ_t$. Do non-dominated sorting for objective rank and crowding distance and assign a rank for each individual (F=F1, F2,…) (Fig. 2).
6. Select the next generation P_{t+1}. An elitist individual is transferred to the next population with a size *Np*.
7. The true objective values are calculated with FEA and then the ranking in steps 4–5 is run once again for the actual values.
8. Steps 1–7 are repeated to generate subsequent generations. The MOGA process is terminated when the stop criterion, such as a predetermined number of generations, is satisfied.
9. The local search is done after the Pareto solution set is obtained. The sequential quadratic programming algorithm in MATLAB® was used as the local optimizer.

It should be noted that in order to utilize the information from constraint violations, the amount of infeasibility (or the extent of constraint violation) was used to rank the solutions. During the first several stages (e.g., n=1–10), the constraint information was utilized to explore more design points near the boundary by keeping those individuals that were found to violate the constraints after obtaining the true objective values by FEA. However, as stated above, with the genetic operation continuing, these points will be automatically eliminated.

It was noted that the proposed method may save a significant amount of computation time. The metamodel generation took approximately 10 h to calculate the design of experiment and model fitting using a HP xw9300 workstation with dual 2.2 GHz AMD Opteron™ Processors and 4 GB of RAM. For example, one genetic operation took 2,440 s. In addition, the objective functions had to be solved 2,777 times in one iteration. This step may only take several hours of calculation calling the Kriging model. Actually, it was a time-consuming process to generate new feasible solutions as noted in the dashed box (Fig. 3). If FEA is used to generate new feasible solutions, each run will last approximately 10 min, and the total time will be 2,777×10=27,770 min or approximately 462.8 h. Moreover, the calculation time using the Kriging model will decrease to about 300 s after the first generation. The savings in computation time will be significant compared to using FEA, especially for problems with a complex boundary in the solution domain.

4.1 Visualization and decision making

The decision for selecting the optimal solution can be obtained with the assistance of visualization. Generally, it is difficult to visualize the established response surface model with six parameters; however, it is possible to visualize the Pareto solution set for any two objectives (in 2-D) or three objectives (in 3-D). In this work, the objectives of corner radius and the tube wall thinning were selected for visualization.

Moreover, visualization can assist to find the global optimum when preference is given for a certain objective. In this paper, it was preferred to obtain a minimum corner radius (or minimum thinning) based on the global multi-objective optimization.

5 Case study: straight tube hydroforming with square-shaped die

5.1 Finite element model

In this section, the load path for hydroforming a straight tube with a 90-mm outer diameter and a 2-mm wall thickness into a square-shaped die was investigated. Figure 4a shows the FE mesh of the die and a deformed tube. Due to the symmetry of the part, only one quarter of the tube and die were modeled for the simulation (Fig. 4a). Figure 4b shows a cross section of the tube inside the die. The forming process consisted of pressurizing and expanding the tube in the radial direction by a distance s until it contacted the die. A compressive force was simultaneously applied at the tube ends to supply more material into the die cavity and thus avoid excessive thinning.

The tube material in this study was mild steel as listed in Table 1, and the hydroforming die was modeled as a rigid body. The tube was meshed with 2,565 Belytschko-Tsay shell elements with seven integration points through the thickness of the tube wall. The material was assumed to be isotropic; therefore, the von Mises yield criterion was used for the simulation. A material model named "MAT_PIECEWISE_LINEAR_PLASTICITY" (No. 24) was chosen to represent the isotropic hardening behavior [26]. Coulomb's coefficient of friction was set to 0.1 for the contact interface.

A mesh sensitivity analysis was completed which included four different mesh sizes: 2, 2.5, 3, and 5 mm. From the resultant deformation of the tube at the A–A cross section (45°) (Fig. 5), it appears that the 2- and 3-mm mesh sizes have a rather symmetric and uniform deformation compared to the 5-mm mesh size. The maximum displacements of the tube are 17.22, 17.77, 16.74, and 16.52 mm for the mesh sizes from 2 to 5 mm, respectively. The displacement for the mesh size of 2.5 mm is much closer (3% difference) to the one for the 2-mm mesh size; however, the former simulation time is only one third of the running time for the 2.0-mm mesh. The optimization was implemented for the 2.5-mm mesh (simulation time of 10 min each run) to evaluate the developed optimization algorithms. Moreover, the simulation and load path optimization with a mesh size of 3 mm and a higher strength steel

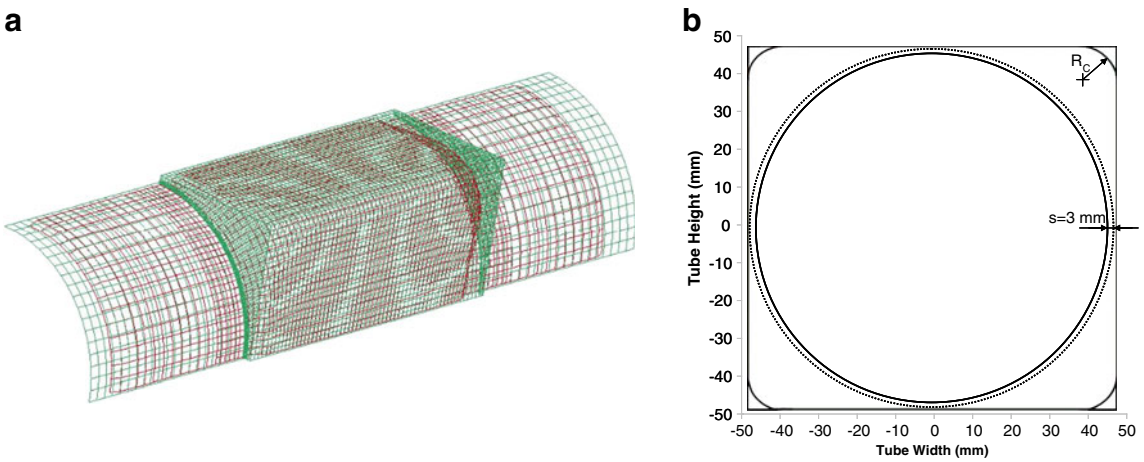

Fig. 4 **a** One quarter of the FE model and **b** geometry of the cross section of die and tube (R_C is the final corner radius of the deformed tube)

(DP600) (Table 1) were completed for a comparison of the results.

5.2 Design variables and objective functions

5.2.1 Design variables

The design variables for the load path were: five parameters for pressure and one for end feed, namely P1, P2, P3, P4, P5, and D (Fig. 6). P1 to P5 were different pressure levels, in megapascal, (P1 was the yield pressure, P2, P3, and P4 were the intermediate pressure levels and P5 was the calibration pressure) and D was the maximum end feed displacement, in mm, at the end of the process. In order to account for different mesh sizes and materials, the ranges for each design variable were selected as follows:

$$\begin{aligned} &10 \le P1 \le 19; \quad 20 \le P2 \le 28; \quad 26 \le P3 \le 28 \\ &30 \le P4 \le 35; \quad 40 \le P5 \le 85; \quad 10 \le D \le 14 \end{aligned} \tag{9}$$

All the design variables and the objective values were linearly normalized between 0.2 and 0.8.

5.2.2 Objective functions and constraints

The load path design for hydroformed parts in which the tube wall fills the corners of a die cavity has two primary objectives: (1) improving the corner-filling ability and (2) minimizing thinning of the tube wall, without reaching the onset of plastic localization. Industrial parts are typically produced in a multi-stage forming process, where a tube is bent and possibly crushed prior to hydroforming. In order to maximize the formability during the final hydroforming stage, the work hardening needs to be minimized in the preliminary stages: the overall level of work hardening can be evaluated by noting the maximum flow stress after forming. Consequently, the maximum stress and strain in the formed part are considered by establishing objective functions in terms of three measures of forming severity: the risk of fracture/necking, wrinkling, and severe thinning.

The forming severity of the hydroforming process was evaluated with both the forming limit diagram (FLD) and the forming limit stress diagram (FLSD) as shown in Fig. 7, where d_f is the minimum distance in stress space from a point (σ_2, σ_1) to the stress limit, and d_{th} is the minimum distance in strain space from a point (ε_2, ε_1) to the thinning limit. Finally, d_w is the distance in stress space from a point (σ_2, σ_1) to the major stress axis, as shown in Fig. 7b.

An objective function to evaluate the risk of necking or fracture was defined as follows [10]:

$$f_1 = \text{Obj\_}f = \frac{1}{d_f} = \frac{1}{\left|\sigma_1^{\max} - k\sigma_f\right|} \tag{10}$$

where σ_1 is the numerically calculated maximum principal stress in element i (i=1 to n, n is the total number of elements in the model) and σ_f is the corresponding forming stress limit

Table 1 Material properties of the tube

Grade	Strength coefficient (MPa)	Yield stress (MPa)	Ultimate tensile stress (MPa)	Density (kg/m^3)	Young's modulus (GPa)	Poisson's ratio	Hardening exponent n
Mild steel	601.8	265	380	7,800	210	0.30	0.168
DP600	795.8	390	610	7,800	205	0.30	0.115

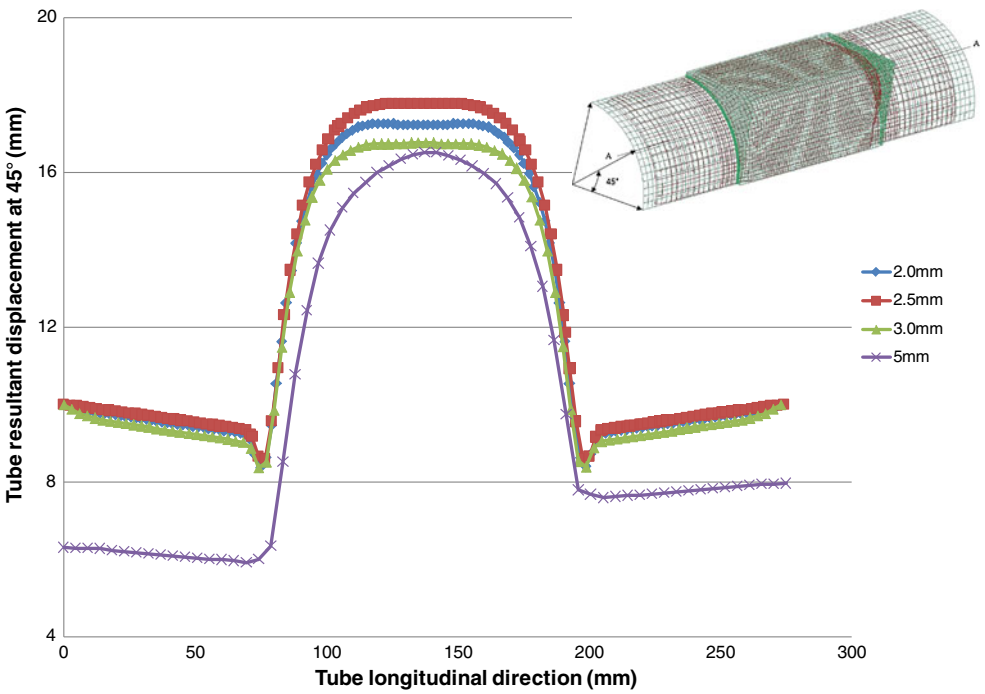

Fig. 5 Comparison of the corner resultant displacement at 45° (cross section A–A) for four different mesh sizes (2, 2.5, 3, and 5 mm)

(Fig. 7b); k is a scaling factor that ensures that σ_1 is not greater than $k\sigma_f$ and is only used to simplify calculations.

An objective function to assess the risk of wrinkling was defined by the following expression:

$$f_2 = \begin{cases} \text{Obj\_}w = \sum_{i=1}^{n} \left|d_w^i\right| = \sum_{i=1}^{n} \left|\sigma_2^i\right| & \sigma_2^i < 0 \\ \text{Obj\_}w = 0 & \sigma_2^i \geq 0 \end{cases} \tag{11}$$

Finally, an objective function was defined to evaluate thinning severity:

$$f_3 = \begin{cases} \text{Obj\_th} = \sum_{i=1}^{n} \left(d_{th}^i\right)^2 & \varepsilon_1^i > \eta\left(\varepsilon_2^i\right) \\ \text{Obj\_th} = 0 & \varepsilon_1^i \leq \eta\left(\varepsilon_2^i\right) \end{cases} \tag{12}$$

where ε_1 is the major strain in element i, and $\eta(\varepsilon_2)$ is the thinning limit d (Fig. 7a). In order to optimize the hydroforming process, the minimum value of each of these objective functions is sought.

The primary objective of the current tube hydroforming problem is to maximize the amount of expansion of the tube wall into the corners of the die, or in other words, to minimize the corner radius:

$$f_4 = R_C \tag{13}$$

The above function (12) of severe thinning was evaluated on every element in the tube. In reality, the local thickness reduction may reach a limit. Hence, the maximum local thinning ratio was employed to minimize the function:

$$f_5 = (t - t_{\min}) \times 100\%/t \tag{14}$$

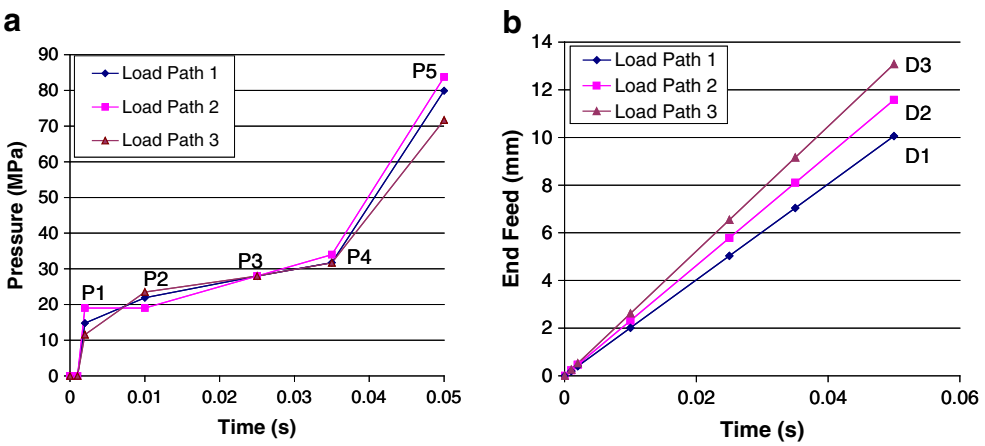

Fig. 6 Load curve for **a** internal pressure and **b** axial end feed displacement

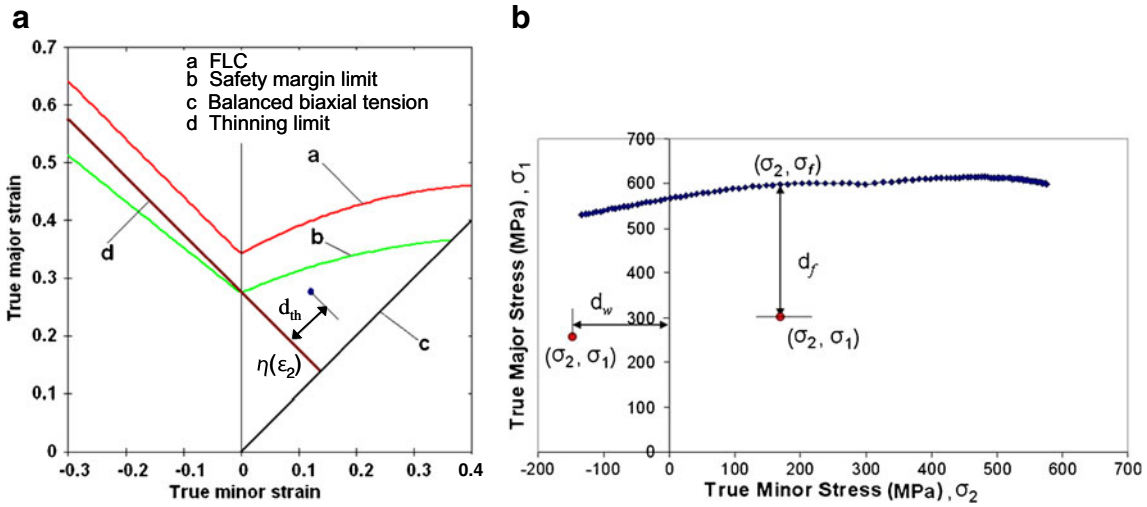

Fig. 7 **a** FLD and **b** FLSD

where t is the original tube thickness, and $t_{\min}$ is the minimum thickness in the deformed tube. The load path is therefore optimized by minimizing each of these formability objectives (Eqs. 10–14), and the problem can be summarized by the following formulation which places constraints on each objective:

$$\begin{aligned} &\text{Minimize} \quad F(x) = [f_1(x), f_2(x), f_3(x), f_4(x), f_5(x)] \\ &st. \quad 0.2 \le f_1 \le 0.75;\ 0.2 \le f_2 \le 0.75 \\ &\qquad 0.2 \le f_3 \le 0.30;\ 0.2 \le f_4 \le 0.60;\ 0.2 \le f_5 \le 0.38 \end{aligned} \tag{15}$$

where x is the normalized vector of design variables: x= [P1, P2, P3, P4, P5, D]^T. After normalization, the range of each design variable is the same: $0.2 \le x_i \le 0.8$, i =1, 2,…6.

It can also be noted that some of these objectives are in conflict with each other in the design domain. Therefore, there will not likely be a single optimal solution that satisfies every objective at the same time.

5.3 Kriging surrogate model

The design of experiments was carried out using the Latin hypercube sampling (LHS) method. The design variables were generated by LHS and normalized within the range [0.2, 0.8]. It has been suggested [25] that the minimum number of design points required to build a quadratic model is $k=d(d-1)/2+3d+1$, where d is the number of factors to analyze. In this case, d= 5 and k=26, but in order to obtain a more precise model 50 design points were generated (Appendix 2).

Then, the tenfold cross-validation was implemented and the PRESS value was obtained for the model with regard to each objective. The data was divided into ten subsets: nine of the subsets were input as the training data and the last one was used as the testing data. The total average error of the cross-validation was obtained as an estimation of the precision.

The quality of the Kriging model is demonstrated by the error and correlation values in Table 2. The PRESS error for each objective was low, and particularly for f_4 which

Table 2 Prediction accuracy of the calculated response surface model for each objective

	f_1	f_2	f_3	f_4	f_5
No. of observations	50	50	50	50	50
PRESS error	0.0040	0.0050	0.0065	0.0008	0.0012
R_{pred^2}	0.9339	0.7408	0.9269	0.9557	0.9611
Syy	0.0606	0.0193	0.0885	0.0186	0.0302

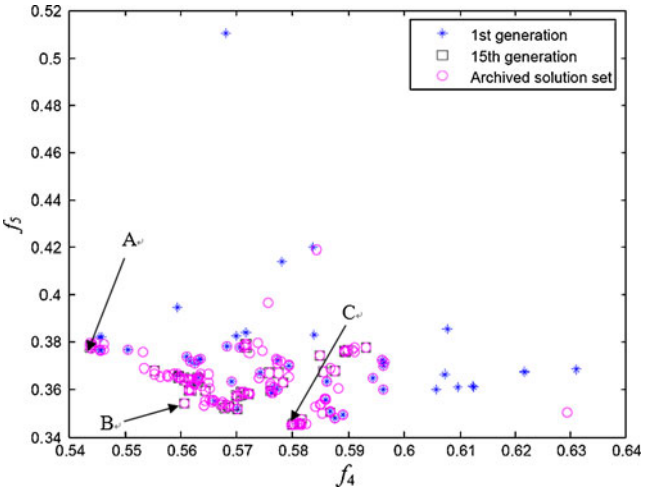

Fig. 8 The evolution of the fourth and fifth objectives (generations 1, 15, and archived set)

Table 3 The objectives of the three selected points (without units)

	f_1	f_2	f_3	f_4	f_5	L2 norm
A (norm)	0.4511	0.5914	0.2078	0.5437	0.3775	0.6619
B (norm)	0.4519	0.4683	0.2001	0.5607	0.3542	0.6632
C (norm)	0.4513	0.6060	0.2000	0.5799	0.3450	0.6748
A (True)	**−98.42**	**260,946**	**0.1629**	**9.1650**	**0.2958**	–
B (True)	**−98.06**	**178,909**	**0.0024**	**9.6198**	**0.2569**	–
C (True)	**−98.32**	**270,663**	**0.0001**	**10.130**	**0.2417**	–

Normalized values and actual objective values (in bold)

norm normalization, *True* FEA results

had the lowest value. Except for objective f_2 (with a value of 74.08%), the Kriging response surface for all the other objectives had a high adjusted coefficient of correlation which indicates an explanation above 92.69% of the variability in predicting new observations. The result for f_2 was a little low, but the value was still reasonable.

6 Results from MOGA and local search algorithms

6.1 Global search using MOGA

The optimization was implemented with MOGA in 15 generations. The elitist chromosomes were saved in an independent archive for each generation. Figure 8 shows three stages in the evolution of the optimization with regard to the fourth and fifth objectives: the 1st generation, the 15th generation, and the final archived solution set. From Fig. 8, it can be seen that both objectives (i.e., the minimum corner radius f_4 and the minimum thinning ratio f_5) evolved efficiently toward the Utopia point, which is defined as point (0,0). The archiving successfully retained the elitist solutions in each generation. Three solutions, including two extreme points and one with the second minimum L_2 norm, were selected for investigation. Table 3 lists the normalized values and actual objective values (in bold).

It can be seen from Table 3 that solution A has the smallest corner radius f_4 or R_C=9.165 mm among the three solutions, but the greatest local thinning ratio (f_5). Solution C has the smallest thinning ratio, but the greatest corner radius R_C=10.13 mm. This indicates that these two objectives (f_4 and f_5) conflict with each other. Moreover, solution B has a larger stress objective value (lower stress safety margin), L_2 norm, and corner radius than solution A, but its thinning (local and global) and wrinkling values are smaller. Generally, it was difficult to determine which solution is better based on just one objective. Therefore, the final decision for the best solution should be made according to the designer's specific criterion or preference. In this paper, the preferred load path was determined by a local search on the basis of the corner radius and the thinning ratio.

If the stress safety margin for this hydroforming process is defined as the difference in major stress between the most critical stress state in the part and the forming limit stress curve, Fig. 9 shows that the optimum safety margin improves after 15 generations. Although the average f_1 value did not vary significantly, the optimum safety margin

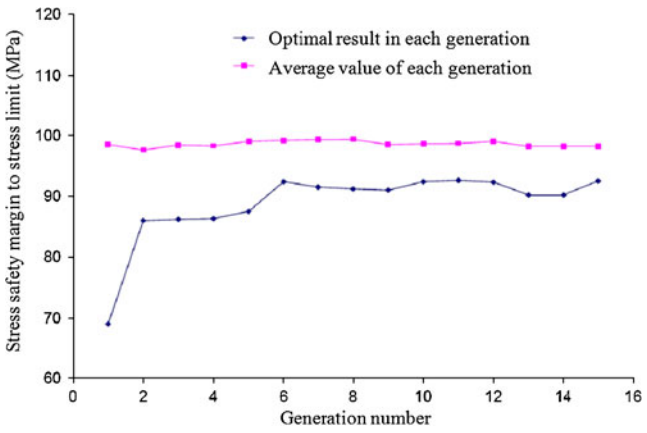

Fig. 9 The evolution of the stress safety margin (*y-axis* absolute value of f1)

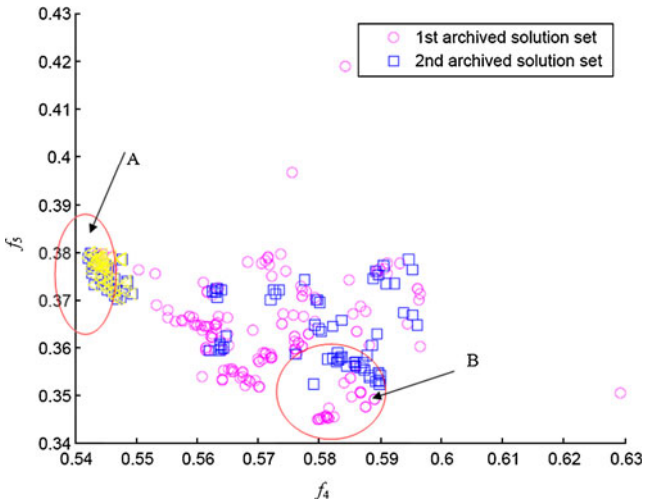

Fig. 10 Comparison of two archived datasets

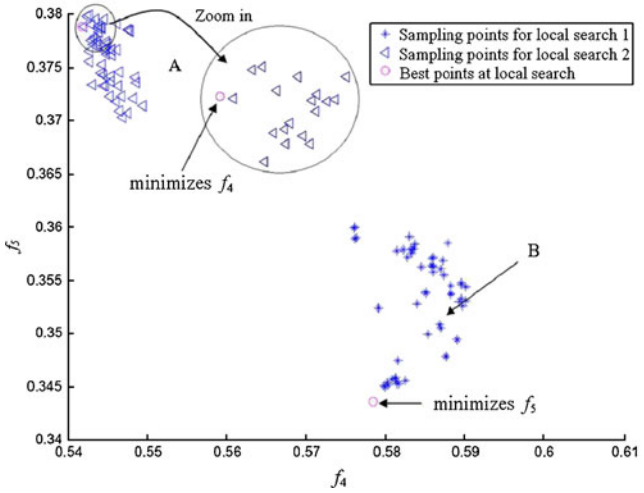

Fig. 11 Best results of local search and sampling points in region A (zoomed in) and region B

increased up to a value of 91 MPa in the last generation. This can be considered an upper limit of the stress safety margin and ensures that the forming process will be robust and will produce quality components.

Therefore, it can be seen that the stress safety margin value improved for the last population as a result of the optimization. In the next step of the local search, it can be assumed that all the design points in the domain nearest the Pareto front have met the formability safety requirements which were represented by the first three objectives.

6.2 Local search using sequential quadratic programming

In the above constraint-handling study, the boundary of the local thinning ratio was relaxed from 0.38 to 0.44 (corresponding to an increase in maximum thinning ratio from 30% to 40%) to investigate the effect of boundary size on the efficiency of the search. A second archived dataset was therefore determined and is plotted in Fig. 10. From the comparison of the two sets shown in Fig. 10, it was verified that the first archived set represents a more uniform distribution and better Pareto solutions (approaching closer to the origin). Nevertheless, it should also be noted that by relaxing the boundary of the thinning ratio objective f_5 improved somewhat (see circled region A in Fig. 10). This means that it is possible to improve the results in this local region where solutions lead to some of the smallest values of the corner radius.

Table 4 Local search result in region A

	f_4	f_5	L2 norm	f_1	f_2	f_3
Local min A$^+$	0.5418	0.3789	0.6619	0.4705	0.4131	0.2057
Global best 1	0.5437	0.3775	0.6619	0.4511	0.5914	0.2078
Global best 2	0.5421	0.3788	0.6613	0.4665	0.6208	0.2069
Local min A$^\Delta$	9.115	0.298	–	−91.35	142,089	0.1187
Global best 1	9.165	0.296	–	−98.42	260,946	0.1629
Global best 2	9.123	0.298	–	−92.72	280,533	0.1467

Table 5 Local search result in region B

	f_4	f_5	L2 norm	f_1	f_2	f_3
Local min B$^+$	0.5785	0.3436	0.6728	0.4508	0.6011	0.2000
Global best 3	0.5799	0.3450	0.6748	0.4513	0.6060	0.2000
Local min B$^\Delta$	10.09	0.2390	–	−98.53	267,381	1.26E−5
Global best 3	10.13	0.2420	–	−98.32	270,663	6.72E−5

Global best 1 and 3 were from the first archived solution set; global best 2 was from the second archived solution set

$^+$ Prediction of local search

$^\Delta$ FEA results of local search

The data from regions A and B (Fig. 10) were used to establish a Kriging response surface model for local search in these two regions, respectively. Only one of the objectives of minimum corner radius (f_4) and local minimum thinning ratio (f_5) were kept as output together with the inputs in the new dataset for setting up the Kriging model. The datasets were extracted from a 361×11 dataset, and each dataset consisted of 50×7 and 55×7 matrices for f_4 and f_5, respectively. The results were plotted inside the circle in Fig. 11.

For the local search in both regions, the local minima were obtained after approximately 40 s of run time. Figure 11 also shows an enlargement of region A where it can be seen that the minimum was slightly better than the value obtained by MOGA. For the local search in region B, there was also a significant improvement: the optimized

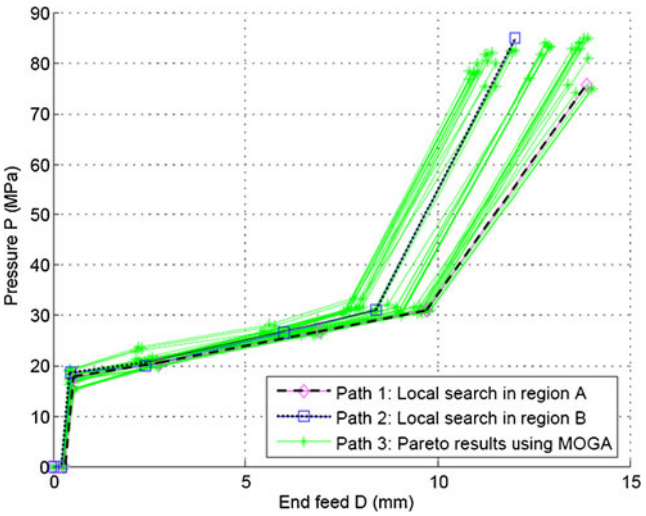

Fig. 12 Comparison of the load path from MOGA and local search

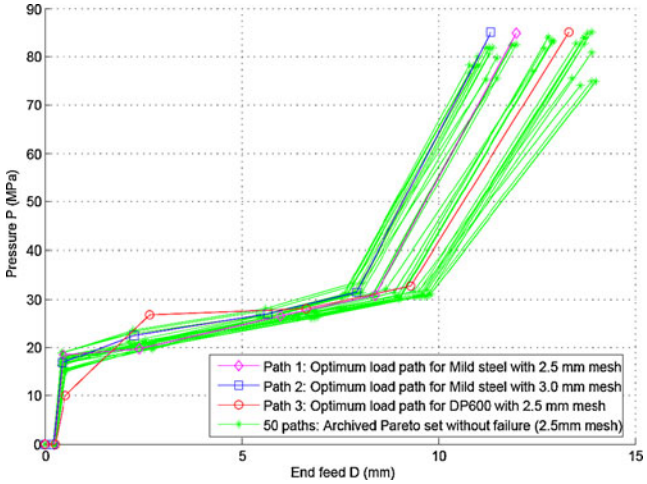

Fig. 13 Comparison of the load paths optimized for different mesh sizes with the mild steel and different material (mild steel and DP600)

results (with "o") were presented and compared to the two archived datasets (shown in Tables 4 and 5). The load paths for these two final minimum objectives and obtained through local searches were plotted and compared with the Pareto load path solutions using MOGA (Fig. 12).

7 Discussion

The predicted results (identified by the symbol +) in the local searches were examined by two additional FEA runs and are also presented in Tables 4 and 5 (identified by the symbol Δ).

Since the solution obtained after the local search was better than that from the MOGA search, the final minimum corner radius was chosen to be 9.115 mm in region A with the preference of a smaller corner radius; meanwhile, the other objective (f_5) under the same load path reached a thinning ratio of 29.8% which is less than 30%. The stress safety margin is 91.35 MPa, which indicates a very safe process. Meanwhile, if less thinning was preferred, the final solution could also be selected from region B, which represents a maximum thinning of 23.9% and a corner radius of 10.09 mm. The results also show that the other objectives improved in terms of the stress safety margin of 98.53 MPa, wrinkling of 267,381 MPa, and thinning value of 1.26e-5.

Table 6 The optimal load path obtained using MOGA

	P1 (MPa)	P2 (MPa)	P3 (MPa)	P4 (MPa)	P5 (MPa)	D (mm)
Load path 1	18.58	19.77	26.50	30.84	84.82	11.99
Load path 2	16.83	22.59	26.97	31.44	85.00	11.34
Load path 3	10.00	26.76	28.00	32.74	85.00	13.31

The above load path results for the mild steel tube were compared with the load paths using a different mesh size and a higher-strength steel DP600 (Fig. 13, Tables 6 and 7). It indicated that the load paths for the finer mesh (2.5 mm) and the coarser mesh (3 mm) were very similar: the pressure difference was only 5.5% (1.2 MPa) and the difference in end feed was only 5.4% (0.65 mm). The maximum pressure and axial end feed are 84.82 vs. 85 MPa and 11.99 vs. 11.34 mm for different mesh size. This verified that this optimization method can generate an accurate result with different mesh sizes. However, the load path for a DP600 tube showed a significantly higher value for the total end feed compared to that for the mild steel tube. In the calibration stage, the rate of pressure increase ($\Delta P/\Delta D$) is almost the same for both tubes, but this is not the case for the early deformation stage. From the observations with different mesh sizes and materials, it underscores the fact that the loading path during the early stages of deformation is more critical to the success of the hydroforming operation than that during the final calibration stage. Therefore, close attention should be paid to the design of the first part of the load path. In Fig. 13, it was shown that the hybrid optimization method is capable to provide a variety of loading paths for design engineers to choose from according to their preference.

8 Conclusions

In this study, a hybrid global and local search optimization strategy was proposed and applied to designing the load path of a hydroformed tubular part with a square cross section. A constraint-handling technique was developed and coupled with the conventional NSGA-II. The following conclusions can be drawn:

1. A constraint-handling algorithm was applied and implemented to the multi-objective optimization with more than three objectives, which incorporated the ranking of constraint violations and a second ranking of non-domination of objectives and local crowding distance.

Table 7 The objectives obtained by current optimal load path

	Final objective results				
	f_1 (MPa)	f_2 (10^5) (MPa)	f_3	f_4 (mm)	f_5 (%)
Optimal path 1	−91	1.42	0.11	9.12	29.80
Optimal path 2	−94	2.43	0	9.79	24.65
Optimal path 3	−1,049	1.39	0.05	13.98	16.49

2. A hybrid algorithm combining the global search (using MOGA) and local search (using SQP) for multi-objective optimization was proposed and applied to the optimization of a hydroformed part. The case study showed better results, with smaller corner radius of 9.115 mm and thickness thinning ratio of 23.9% being obtained compared to the single MOGA search with corner radius of 10.09 mm and thinning ratio of 29.8% up to 9.7% and 19.8% improvement, respectively.
3. The optimization problem with five objectives was investigated first. It was noted that the proposed method, which uses the Kriging predictor to generate new points, with constraint handling and FE calculation for evaluating new offsprings can achieve a good performance in terms of both accuracy and efficiency in dealing with more than three objectives.
4. Visualization was used to assist in decision making and to search for the Pareto solutions. It is suggested that the plotting of results be focused on the preferred objectives.
5. This case study showed that the stress safety margin improved when the corner filling and thinning objectives were attained. The improved stress safety margin leads to a more robust forming process and a better quality part.

Acknowledgments The authors would like to acknowledge the financial support of the Natural Sciences and Engineering Research Council of Canada (NSERC–Canada Research Chair 202632) and the Ontario Graduate Scholarship in Science and Technology (OGSST) in Canada.

Appendix 1

Table 8 The example of the evolution in generation=1 sorting by constraint violation (CV) operation in constrained MOGA

Columns 10 through 15 of the constraint violation output					
f_4	f_5	Non-dominated sorting	Crowding distance	Violation value	Rank of violation
0.5844	0.4190	1.0000	Inf	0	1.0000
0.5632	0.3724	1.0000	0.3742	0	1.0000
0.5755	0.3968	1.0000	0.2165	0	1.0000
0.5763	0.3589	1.0000	0.1681	0	1.0000
0.5455	0.3767	1.0000	0.0832	0	1.0000
0.5464	0.3928	1.0000	0.2603	0	1.0000
0.5794	0.3700	1.0000	0.1218	0	1.0000
0.5992	0.4181	2.0000	0.5982	0	1.0000
0.5658	0.4567	2.0000	0.7687	0.0067	2.0000
0.6107	0.3618	1.0000	0.3514	0.0107	3.0000
.	.	.	.	.	.
.	.	.	.	.	.
.	.	.	.	.	.
0.7224	0.3636	1.0000	Inf	0.1224	28.0000
0.7543	0.4788	2.0000	Inf	0.1831	29.0000
0.7451	0.5010	2.0000	Inf	0.1961	30.0000
0.5807	0.5628	3.0000	5.0000	0.2127	31.0000
0.5515	0.5543	2.0000	0.4206	0.2191	32.0000
0.5275	0.5659	2.0000	0.7948	0.2280	33.0000
0.5410	0.5674	1.0000	1.3884	0.2321	34.0000
0.5101	0.5394	2.0000	0.9650	0.2663	35.0000

Appendix 2

Table 9 The dataset of DOE with LHS: input of 6 and output of 5 (normalized)

No.	P1	P2	P3	P4	P5	D	f_1	f_2	f_3	f_4	f_5
1	0.6639	0.5962	0.3524	0.2555	0.6074	0.4228	0.4541	0.5308	0.2061	0.5992	0.4181
2	0.3906	0.4206	0.3929	0.5785	0.4020	0.4409	0.4183	0.6249	0.2031	0.6474	0.3771
3	0.3989	0.7203	0.3890	0.7760	0.4858	0.2255	0.7132	0.6199	0.6168	0.5244	0.5749
4	0.2839	0.7635	0.2360	0.6522	0.4508	0.6988	0.7152	0.4571	0.6347	0.5567	0.5746
5	0.5243	0.3993	0.6000	0.5907	0.2053	0.2092	0.3847	0.6165	0.2003	0.7223	0.3636
6	0.6258	0.3054	0.2908	0.6836	0.5655	0.3956	0.4369	0.4505	0.2011	0.6390	0.3757
45	0.2622	0.3839	0.5328	0.6208	0.3679	0.6356	0.4232	0.5950	0.2047	0.6601	0.3885
46	0.3817	0.3953	0.4032	0.3336	0.3152	0.2334	0.4017	0.5873	0.2012	0.6803	0.3654
47	0.2747	0.7993	0.4086	0.4053	0.2068	0.3165	0.6611	0.4954	0.6230	0.6230	0.5606
48	0.6355	0.7375	0.6964	0.6363	0.7951	0.5106	0.6780	0.5495	0.4518	0.5188	0.5670
49	0.4592	0.3053	0.7641	0.2841	0.7943	0.7835	0.4810	0.4883	0.2017	0.5631	0.3724
50	0.7428	0.3632	0.3917	0.2727	0.7848	0.6370	0.4521	0.5992	0.2074	0.5455	0.3766

DOE design of experiment

References

1. Manabe K, Amino M (2002) Effects of process parameters and material properties on deformation process in tube hydroforming. J Mater Process Technol 123:285–291
2. Yang JB, Jeon BH, Oh SI (2001) Design sensitivity analysis and optimization of the hydroforming process. J Mater Process Technol 113:666–672
3. Fann KJ, Hsiao PY (2003) Optimization of loading conditions for tube hydroforming. J Mater Process Technol 140:520–524
4. Imaninejad M, Subhash G, Loukus A (2005) Load path optimization of tube hydroforming process. Int J Mach Tool Manufact 45:1504–1514
5. Lorenzo RD, Filice L, Umbrello D, Micari F (2004) Optimal design of tube hydroforming processes—a fuzzy-logic-based approach. Proc Inst Mech Eng B J Eng Manuf 218(6):599–606
6. Ray P, Donald BJM (2004) Determination of the optimal load path for tube hydroforming processes using a fuzzy load control algorithm and finite element analysis. Finite Elem Anal Des 41 (2):173–192
7. Koç M, Allen T, Jiratheranat S, Altan T (2000) The use of FEA and design of experiments to establish design guidelines for simple hydroformed parts. Int J Mach Tool Manufact 40:2249–2266
8. Ingarao G, Lorenzo RD, Micari F (2009) Internal pressure and counterpunch action design in Y-shaped tube hydroforming processes—a multi-objective optimisation approach. Comput Struct 87:591–602
9. Bonte MHA, van den Boogaard AH, Huétink J (2008) An optimisation strategy for industrial metal forming processes, modelling, screening and solving of optimisation problems in metal forming. Struct Multidiscip Optim 35:571–586
10. An H, Green DE, Johrendt J (2010) Multi-objective optimization and sensitivity analysis of tube hydroforming simulations. Int J Adv Manuf Technol 50(1–4):67–84. doi:10.1007/s00170-009-2505-x
11. An H, Green DE, Johrendt J (2009) A global optimization of load path design for tube hydroforming applications using MOGA, IDDRG conference, June, Golden, CO, USA, 307–318
12. Hughes EJ (2005) Evolutionary many-objective optimisation: many once or one many? In: 2005 IEEE Congress on Evolutionary Computation (CEC'2005), vol. 1. IEEE Computer Society Press, Los Alamitos, pp 222–227
13. Goel T, Vaidyanathan R, Haftka RT, Shyy W, Queipo NV, Tucker K (2007) Response surface approximation of Pareto optimal front in multi-objective optimization. Comput Meth Appl Mech Eng 196:879–893
14. Myers RH, Montgomery DC (1995) Response surface methodology—process and product optimization using designed experiment, Wiley-Interscience
15. Hussain MF, Burton RR, Joshi SB (2002) Metamodeling: radial basis functions, versus polynomials. Eur J Oper Res 138:142–154
16. Karkoub MA, Elkholy AH, Al-Hawaj OM (2002) Modelling deformation of hydro-formed circular plates using neural networks. Int J Adv Manuf Technol 20:871–882
17. Lophaven SN, Nielsen HB, Søndergaard J (2002) DACE—a Matlab Kriging toolbox, Version 2.0, Technical Report IMM-REP-2002-12 *Informatics and Mathematical Modelling*, Technical University of Denmark
18. Goovaaerts P (1997) Geostatistics for natural resources evolution. Oxford University Press, New York, NY
19. Sacks J, Welch WJ, Mitchell TJ, Wynn HP (1989) Design and analysis of computer experiments. Stat Sci 4(4):409–435
20. Deb K, Pratap A, Agarwal S, Meyarivan T (2002) A fast and elitist multiobjective genetic algorithm: NSGA-II". IEEE Trans Evol Comput 6(2):182–197
21. Konak A, Coit DW, Smith AE (2006) Multi-objective optimization using genetic algorithms: a tutorial. Reliab Eng Syst Saf 91:992–1007
22. Wang J and Yin Z (2008), C-NSGA-II-MOPSO: an effective multi-objective optimizer for engineering design problems, Chapter 4 in Book: global design to gain a competitive edge,519-528, Springer London. doi:10.1007/978-1-84800-239-5
23. Favuzza S, Ippolito MG, Sanseverino ER (2006) Crowded comparison operators for constraints handling in NSGA-II for optimal design of the compensation system in electrical distribution networks. Adv Eng Informatics 20:201–211
24. Seshadri A (2006), multi-objective optimization using evolutionary algorithms (MOEA), Matlab website: http://www.mathworks.com/matlabcentral/fileexchange/10429, by 19 Mar (Updated 27 Jan 2009), accessed on March 8, 2009
25. Mehnen J, Michelitsch T, Lasarczyk C, Bartz-Beielstein T (2007) Multi-objective evolutionary design of mold temperature control using DACE for parameter optimization. Int J Appl Electromagn Mech 25:661–667
26. Hallquist JO (2007), LS-DYNA. Keyword User's Manual, Ver. 971. LSTC